



HAL
open science

Stability of rift axis magma reservoirs: Spatial and temporal evolution of magma supply in the Dabbahu rift segment (Afar, Ethiopia) over the past 30 kyr

S. Medynski, Raphaël Pik, Pete Burnard, C. Vye-Brown, Lyderic France, Irene Schimmelpfennig, K. Whaler, N Johnson, Lucilla Benedetti, D Ayelew, et al.

► **To cite this version:**

S. Medynski, Raphaël Pik, Pete Burnard, C. Vye-Brown, Lyderic France, et al.. Stability of rift axis magma reservoirs: Spatial and temporal evolution of magma supply in the Dabbahu rift segment (Afar, Ethiopia) over the past 30 kyr . Earth and Planetary Science Letters, 2015, 409, pp.278-289. 10.1016/j.epsl.2014.11.002 . hal-01469936

HAL Id: hal-01469936

<https://amu.hal.science/hal-01469936>

Submitted on 22 Feb 2017

HAL is a multi-disciplinary open access archive for the deposit and dissemination of scientific research documents, whether they are published or not. The documents may come from teaching and research institutions in France or abroad, or from public or private research centers.

L'archive ouverte pluridisciplinaire **HAL**, est destinée au dépôt et à la diffusion de documents scientifiques de niveau recherche, publiés ou non, émanant des établissements d'enseignement et de recherche français ou étrangers, des laboratoires publics ou privés.

Stability of rift axis magma reservoirs: Spatial and temporal evolution of magma supply in the Dabbahu rift segment (Afar, Ethiopia) over the past 30 kyr

S. Medynski^{a,*}, R. Pik^a, P. Burnard^a, C. Vye-Brown^b, L. France^a, I. Schimmelpfennig^c, K. Whaler^d, N. Johnson^d, L. Benedetti^c, D. Ayelew^e, G. Yirgu^e

^a CRPG UMR 7358 CNRS, Université de Lorraine, 15 rue Notre Dame des Pauvres, 54500 Vandoeuvre-lès-Nancy, France

^b British Geological Survey, Murchison House, West Mains Road, Edinburgh, EH9 3LA, United Kingdom

^c Aix-Marseille Université, CNRS-IRD-Collège de France, UM 34 CEREGE, Aix-en-Provence, France

^d University of Edinburgh, The King's Buildings West Mains Road, Edinburgh, EH9 3JW, United Kingdom

^e School of Earth Sciences, Addis Ababa University, Ethiopia

Keywords:

continent–ocean transition

focussed/unfocussed magmatism

diking

cosmogenic ³⁶Cl and ³He

Unravelling the volcanic history of the Dabbahu/Manda Hararo rift segment in the Afar depression (Ethiopia) using a combination of cosmogenic (³⁶Cl and ³He) surface exposure dating of basaltic lava-flows, field observations, geological mapping and geochemistry, we show in this paper that magmatic activity in this rift segment alternates between two distinct magma chambers. Recent activity in the Dabbahu rift (notably the 2005–2010 dyking crises) has been fed by a seismically well-identified magma reservoir within the rift axis, and we show here that this magma body has been active over the last 30 kyr. However, in addition to this axial magma reservoir, we highlight in this paper the importance of a second, distinct magma reservoir, located 15 km west of the current axis, which has been the principal focus of magma accumulation from 15 ka to the subrecent. Magma supply to the axial reservoir substantially decreased between 20 ka and the present day, while the flank reservoir appears to have been regularly supplied with magma since 15 ka ago, resulting in less variably differentiated lavas. The trace element characteristics of magmas from both reservoirs were generated by variable degrees of partial melting of a single homogeneous mantle source, but their respective magmas evolved separately in distinct crustal plumbing systems.

Magmatism in the Dabbahu/Manda Hararo rift segment is not focussed within the current axial depression but instead is spread out over at least 15 km on the western flank. This is consistent with magneto-telluric observations which show that two magma bodies are present below the segment, with the main accumulation of magma currently located below the western flank, precisely where the most voluminous recent (<15 ka) flank volcanism is observed at the surface.

Applying these observations to slow spreading mid-ocean ridges indicates that magma bodies likely have a lifetime of a least 20 ka, and that the continuity of magmatic activity is maintained by a system of separate relaying reservoirs, which could in return control the location of spreading. This long term (>10⁵ yr) alternation between distinct crustal reservoirs located broadly at the same location relative to the segment appears to be a key feature for organizing and maintaining active spreading centres over stable soft points in the mantle.

1. Introduction

Extension constitutes a major feature of plate tectonics, mainly expressed at mid-oceanic ridges (MOR) and continental rifts. In both marine and subaerial rifting environments, tectonic and magmatic processes (e.g. faulting and dyking) interact in various proportions to accommodate extension, depending on the maturity of the rifting system (e.g. early continental rifting stage,

Abbreviations: DMH, Dabbahu/Manda Hararo; MRS, Magmatic Rift Segment; TCN, Terrestrial TCN; COT, Continent–Ocean Transition; MSMC, Mid-Segment Magma Chamber.

* Corresponding author.

E-mail address: smsorcha@gmail.com (S. Medynski).

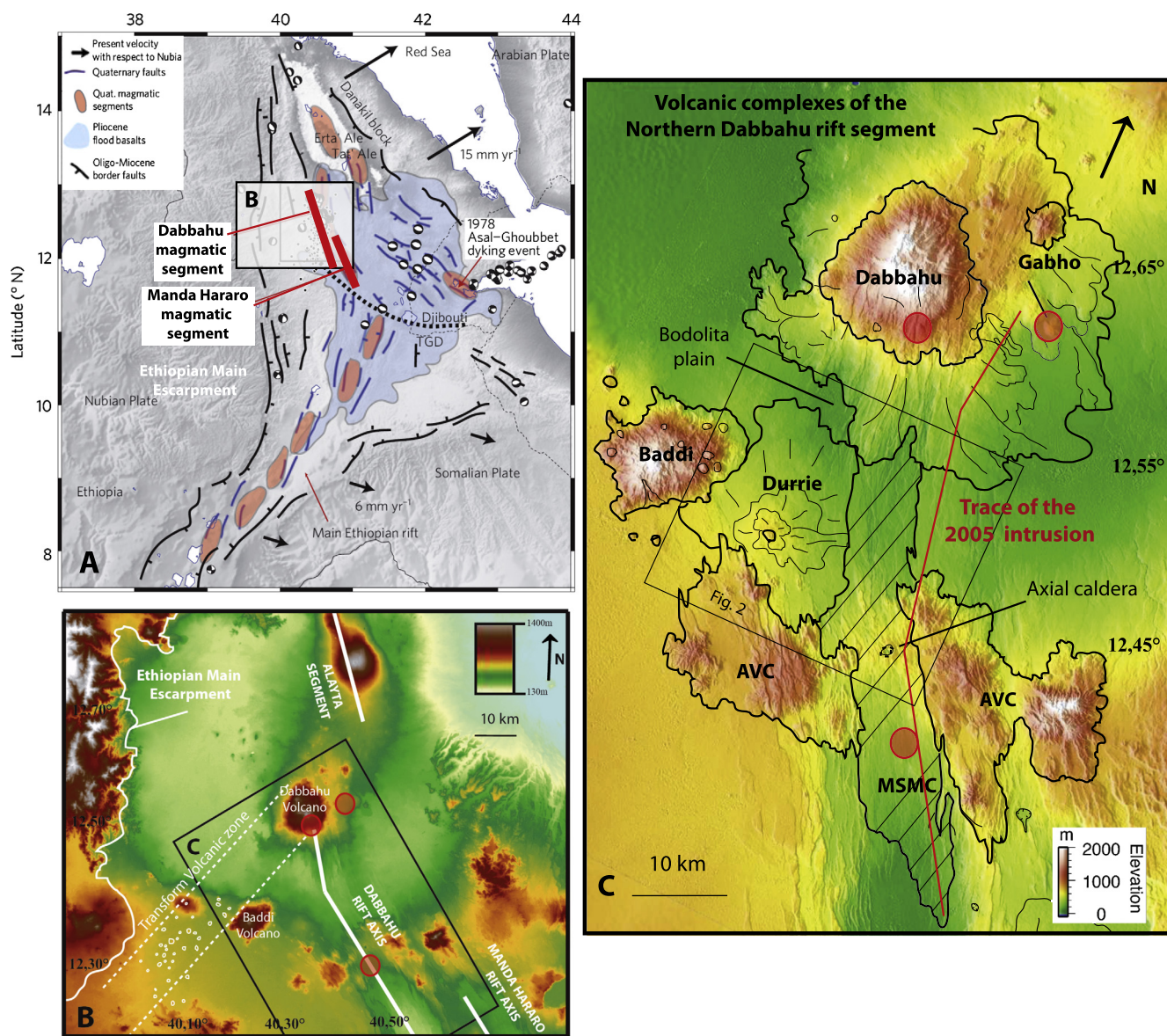


Fig. 1. A: Regional topography of the Afar region (after Hayward and Ebinger, 1996). Active magmatic segments are in red. **B:** Regional topography of the DMH segment and its relation with the Alayta segment and the Transform Volcanic Zone. **C:** Detail of the DMH segment and the extent of volcanic products issued from the volcanic complexes of the rift. AVC is the Ado-Ale Volcanic Complex and MSMC is for the mid-segment magma chamber which feeds the current rift axis (striped area). Note the small Durrie volcano, on the western flank of the rift, between the AVC, the Badi volcano and the rift axis.

ocean–continent transition stage or mature oceanic ridge stage) and the along-axis distribution of magma at the segment scale (Ebinger and Hayward, 1996; Standish and Sims, 2010; Colman et al., 2012). The development of a magma plumbing system and rift architecture that are stable through time remains poorly documented at ridge settings due to the inaccessibility of mid-ocean ridges (MOR) and the resulting lack of chronological constraints on the magmatic processes.

The Afar triple junction, Ethiopia, has often been taken as an analogue of a mature oceanic spreading centre as, being sub-aerial, it is more accessible than MOR (Ebinger and Hayward, 1996; Hayward and Ebinger, 1996). Even if the process of formation of oceanic crust in the Afar is not entirely complete with respect to the nature of the crust (Bastow and Keir, 2011; Hammond et al., 2011), this area allows the morphological evolution of individual rift segments to be studied directly. Additionally, the Dabbahu/Manda Hararo (DMH) segment, in the western Afar (Fig. 1A), has been intensively studied following a major rifting crisis which began in 2005 and affected the northern half (Dabbahu sec-

tion) of the DMH rift (Wright et al., 2006; Ayele et al., 2009; Ebinger et al., 2010; Ferguson et al., 2010; Grandin et al., 2010a, 2010b). This crisis allowed the magmatic reservoirs responsible for successive shallow intrusions to be identified, and the topographic response induced by successive dike intrusions over the period 2005–2010 to be quantified (Wright et al., 2006; Ayele et al., 2007, 2009; Grandin et al., 2009; Keir et al., 2009; Ferguson et al., 2010; Belachew et al., 2011; Keir et al., 2011; Desissa et al., 2013; Fig. 1B and detail in Fig. 1C). However, several unsolved questions remain concerning how rift topography develops. For example, the role exerted by individual magma reservoirs remains debated, due to a lack of constraints on parameters such as their replenishment/recurrence time, or the persistence of their spatial distribution particularly over timescales ranging from 10^3 to 10^5 yr. These questions are fundamental for understanding how magmatic accretion can be sustained by either ephemeral or long-lived magma chambers and on which timescale MOR morphology is acquired (Macdonald, 2001). According to Ferguson et al. (2013) the DMH rift already presents focussed magmatic activity (i.e. limited to the

axial depression) as is the case in mature oceanic ridges. However, recent magneto-telluric measurements have shown that a massive magma body is present in the crust and upper mantle in a slightly off-axis position (West of the axial magma chamber), representing at least 500 km³ of magma encompassing a depth range of about 15–30 km (Desissa et al., 2013). This magma volume is large enough to feed about 100 episodes of the magnitude of the 2005 event (Buck, 2013). The location of this magma body, if active, is inconsistent with “focussed” magmatic activity at the DMH rift segment.

In this study, we combine geological mapping of surface topography, structure and lava architecture, major and trace element analyses and cosmogenic ³⁶Cl and ³He exposure dating of lavas erupted along an East/West transect of the DMH rift segment (Figs. 1 and 2). The aim of this work is to assess the stability of the magmatic reservoirs in a rifting environment.

2. Geological setting

The Afar region forms the junction between three extensional systems: the Gulf of Aden Ridge, the Red Sea Ridge and the Main Ethiopian Rift (Fig. 1A). The separation of the Nubian and Arabian plates led to the creation of the triangular Afar depression, cutting into a massive pile of continental flood basalts (CFB), emplaced around 30 Ma ago (Hofmann et al., 1997) and linked to the activity of an underlying plume (Marty et al., 1996; Pik et al., 2006; Bastow et al., 2008). The rifting stage of the Red Sea Ridge started 29–25 Ma ago (Wolfenden et al., 2005), and since 2–1 Ma the rift segmentation has been organized along four en-échélon principal magmatic rift segments (MRS): Erta’ Ale, Tat’ Ale, Alayta and Dabbahu/Manda Hararo (DMH) (Figs. 1A and 1B). Those MRS are typically 60–100 km long and 20–40 km wide, associated with highly faulted differentiated volcanoes (Lahitte et al., 2003; Barberi et al., 1972; Field et al., 2012; Rowland et al., 2007).

The current spreading rate for Afar obtained by geodetic data is ~15 mm/yr (Calais et al., 2006; McClusky et al., 2010), comparable to that of Iceland and other slow spreading ridges (Macdonald, 2001; Carbotte, 2005). However, complete continental break-up has not yet occurred in the Afar, resulting in a stretched and heavily intruded crust (Tiberi et al., 2005; Bastow et al., 2010; Hammond et al., 2012) more akin to the continent–ocean transition (COT) stage than to a mature oceanic spreading centre.

Morphologically, the DMH spreading centre can be subdivided into two sub-segments: the Manda Hararo segment in the south, and the active Dabbahu segment in the North (Fig. 1A and B). The current morphology of the Manda Hararo segment has likely been in place since 220 ka and was active until at least ~31–39 ka at the axis (Lahitte et al., 2003). It seems likely, however, that volcanic activity more recent than this has occurred in the Manda Hararo segment as unweathered lava flow tops and a lack of cover by aeolian sediments (similar to surfaces of young dated lavas in the Dabbahu segment) have been observed (Ferguson et al., 2010; Medynski et al., 2013), which implies <~5 kyr activity. The transition between these two sub-segments is characterized by a shift of the axial depression to the west (Fig. 1A and B). The Dabbahu sub-segment – which steps to the west relative the Manda Hararo segment – is about 60 km long, and presents an axial rift valley of ~40 to 100 m deep. Its last recorded volcanic activity was linked to the 2005 rifting event, with the emission of fissure lavas in 2007, 2009 (Ferguson et al., 2010) and 2010. The rift axis cuts the rhyolitic and at present undated Ado-Ale Gommoyta volcanic complex (AVC) in the middle of the segment (Fig. 1C). There is a small caldera in an elevated section of the rift (about 1 km diameter) present at the intersection of the rift (Dabbahu segment) with the AVC. This portion of the rift segment is characterized by a complex fault pattern (Rowland et al., 2007), associated with a

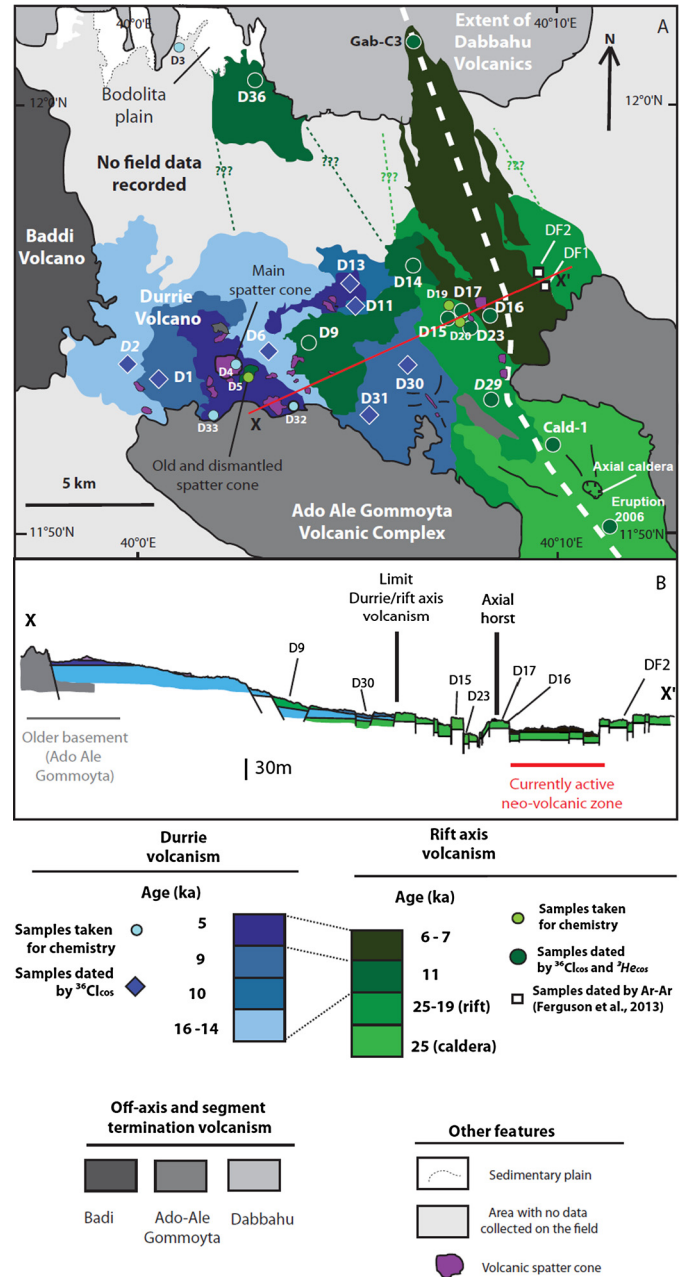


Fig. 2. A: Detailed map of the area studied with sample locations. Small circles denote samples analysed for chemistry alone. Large circles and diamonds were also dated by cosmogenic nuclides. Lava surfaces are colored as a function of their eruptive location (rift flanks/rift axis): blue represents flank volcanism, whereas green represents volcanism from the current neo-volcanic zone; volcanic spatter cones are in purple. Chemical analyses show that some flank lavas present the chemical characteristics of the rift axis lavas (discussed in the text). As a result, the corresponding flow fields are marked in green (= rift affinity) despite the fact that they are geographically located on the adjoining flank. DF-1 and DF-2 (squares) are from Ferguson et al. (2013) and were dated by the Ar-Ar technique. The boundaries of these lava flow fields (a flow field can encompass multiple indistinguishable lava flows) are defined by a combination of mapping (including remote sensing data), field observations, age determinations and chemical data. **B:** Topographic profile (from the Lidar DEM of the NERC-funded Afar Rift Consortium, courtesy of Barbara Hoffman) along the transect, showing the topographic influence of the Durrie flank volcano on the rift morphology. Note that the limit between Durrie volcanism and the rift axis is controlled by pre-existing topography (see the normal West-dipping fault between samples D-15 and D-30). Also note that the contact with the axial/Durrie volcanism and the basement (most likely the dissected Ado-Ale volcanic complex) is hypothetical, because it does not outcrop in the field. For more details on the mapping of the North of the segment – e.g. the contact zone with the Dabbahu volcanics – please see Medynski et al. (2013). For more details on the mapping in unsampled areas, please see Vye-Brown et al. (2012).

re-orientation of the axial depression. South of the caldera, the axial rift valley is oriented NW–SE, whereas further north the faults reorient toward the Dabbahu volcano in an NNW–SSE direction (Fig. 1C).

The northern extremity of the segment is marked by the presence of Dabbahu volcano, a strato-volcano supplied by series of stacked sill-like magma reservoirs (Field et al., 2012), which produced lavas from 72 ka (Medynski et al., 2013) to 5 ka ago (Field et al., 2013). This composite volcano forms the northern end of an NE–SW alignment of numerous volcanic centres and eruptive fissure vents that define a transform volcanic zone (Fig. 1B). This volcanic transform zone is Pleistocene in age (Lahitte et al., 2003; Ferguson et al., 2013) and extends SW to the Ethiopian escarpment (Fig. 1A).

On the western flank (between the rift axis, the western part of the AVC and Badi volcano – Fig. 1) stands the small Durrie volcanic complex which overlaps the previous topography. The central portion of the rift (including the Durrie volcanic complex) is characterized by the emission of pāhoehoe lavas (Vye-Brown et al., 2012, submitted for publication; Vye-Brown, 2012).

Recent magneto-telluric studies show that two low resistivity zones are present at depth below the DMH segment, which most likely correspond to magma reservoirs, one at about 10 km, the other between 15 and at least 30 km depth, suggesting that magma storage beneath the rift axis is composite and not restricted to a single reservoir (Desissa et al., 2013). The first, axial reservoir matches the position of the mid-segment magma chamber as recorded by the seismic activity during dike injections (Keir et al., 2009; Grandin et al., 2009; Belachew et al., 2011; Ebinger et al., 2008). The second, larger reservoir, is located slightly off-axis, between the current rift axis and the Badi volcano (Desissa et al., 2013) directly below the Durrie volcanic complex.

In this study we focus on a transect extending across the mid-segment part of the Dabbahu segment from the axis to the west. This section of the DMH rift lacks temporal constraints on tectonic and/or magmatic activity with the exception of sparse Ar–Ar dating of lavas on the easternmost shoulder of the rift (Ferguson et al., 2013).

3. Mapping details

The area studied covers ~270 km² between the rift mid-axis and the Badi volcano (Figs. 1 and 2) on the western flank. This region is beyond the influence of Dabbahu volcano (15 km to the north), which controls topography acquisition in the northern extremity of the MRS (Medynski et al., 2013).

On the western flank, 10 km from the present-day axis, stands a small flank volcano, Durrie, which is characterized by a central spatter cone surrounded by numerous (>20) smaller cones distributed over the rift flank. The lava flow fields erupted from the flank cones spread over ~160 km² (Fig. 2). This volcanism resurfaced the western rift margin (the term “resurfacing” is used to indicate a period of volcanic activity sufficiently intense to erase the underlying topography, for example, by completely infilling the axial valley): the topographic profile (Fig. 2B) and the geological map (Fig. 2 and Vye-Brown et al., 2012, submitted for publication) show that the density of faults diminishes in the vicinity of the Durrie volcano, which was also confirmed by field observations.

In order to focus sampling on relevant morphological objects relative to rift topography acquisition and the different volcanic complexes, the methods, software and manipulation of spectral images used to produce the new geological map of the DMH Rift (Vye-Brown et al., 2012) were applied. In this portion of the rift, only lobate pāhoehoe lava flows outcrop, making lava unit contacts difficult to distinguish in the field. Moreover, the petrologic

textures of the lavas are similar, with microlithic assemblages of clinopyroxenes and plagioclases (and rare olivine), further complicating identification of individual units. In this situation, remote sensing techniques (Landsat, ASTER, and LiDAR; see SOM 1) can be used in order to distinguish the different lava flow units (Vye-Brown et al., submitted for publication).

4. Sampling details

Between 12 to 15 different eruptive units were identified on Durrie based on remote sensing and field-based data, whereas only 3 units are distinguishable in the axial valley, likely due to stacking of lavas in the depression: the limited surface available for lava expansion implies more efficient resurfacing in the axial valley than on the rift flanks where lava flows can spread radially. Sample locations, carefully selected in order to be representative of the flow units identified from the detailed mapping, are reported in Fig. 2, and sample details are summarized in Table 1. All 24 lava flow samples described here were analysed for chemical composition (major and trace elements). In addition, 15 lava flow samples were dated using cosmogenic ³⁶Cl (see SOM 2) and two others were dated with cosmogenic ³He, following the protocol described in Medynski et al. (2013) (D-2 and D-29).

4.1. Flank volcanism samples

The Durrie volcanic cones and lavas are composed of piled pāhoehoe flows, mainly focused around the 40 m high central spatter cone (Fig. 2A, Table 1 for sample details). Samples D-9 and D-14 are part of the same eruptive unit, which flows down-slope on the eastern flank of the Durrie main spatter cone, clearly identified by remote sensing as a single flow field with a distinct contact with adjacent flow fields visible on the high resolution SPOT DEM (see SOM 1). This unit was sampled at its two extremities (Fig. 2) in order to test the homogeneity of exposure ages on the same unit, and also to validate the mapping by geochemistry. Sample D-4, taken from the top of the main Durrie spatter cone, and sample D-5, part of a pre-existing, partly dismantled cone (Fig. 2), were not suitable for dating but were analysed for chemistry. Sample D-3 was taken from the northern flank-unit (see Fig. 2) was also unsuitable for dating, and is therefore only used here for comparative chemistry. Samples D-32 and D-31, from the upper units of the Durrie cone, were only intended for chemical analyses (not dated).

4.2. Rift axis volcanism

The studied portion of the rift axis is characterized by a horst with a well-preserved volcanic cone (Fig. 2B). East of this horst lies the main rift axis depression, partially in-filled by extremely low albedo (i.e. recent) lavas. On the western side of the horst, a deep, narrow depression (30–40 m deep, 1–2 km wide) extends (with an NW–SE orientation) up to an axial caldera (~10 km SE of the axial horst, at the intersection with the AVC) (Fig. 2). Several fissure vents can be observed in the depression between the horst and the caldera. Lava flows are piled up in a monotonous sequence, characterized by the presence of a massive and thick (>4 m) dolerite lava layer (Fig. 3). This dolerite layer outcrops in the field at the base of the main faults, spreading over several hundred meters, and recurs several times along the rift depression. The dolerite layer is thick and laterally extensive; flows emplaced after this are generally thinner, and the height of the surrounding pāhoehoe lava pile gradually decreases away from the horst cone (Fig. 3), suggesting that the dolerite layer represents the initial stage of an intense volcanic period. It was sampled at the axis (sample D-20, see Fig. 2) in order to compare its chemical characteristics with other lava units.

Table 1
Sample labels and details for all samples analysed here. Those given in italics were analysed for chemistry alone. Samples in regular font were dated by the cosmogenic ^{36}Cl technique, and those in bold using cosmogenic ^3He .

	Latitude (°N)	Longitude (°E)	Altitude (m)	Geomorphology	Distance to rift axis (km) ^a	Petrology	Exposure age (ka)	± (1σ)
Durrie volcano lavas								
D1	12°22.148'	40°26.732'	574	pahoehoe lava top	13	Basalt	8.9	1.1
D2	12°22.844'	40°26.359'	554	pahoehoe lava top	13.2	Basalt	14.5	3.6
D6	12°22.780'	40°29.382'	560	pahoehoe lava top	8.2	Basalt	14.9	1.5
D4	12°22.482'	40°28.650'	599	<i>spatter cone</i>	10	<i>Basalt</i>		
D5	12°22.425'	40°28.700'	591	<i>spatter cone</i>	10	<i>Basalt</i>		
D9	12°23.483'	40°30.255'	466	pahoehoe lava top	6.5	Basalt	11.6	1.2
D14	12°24.385'	40°32.013'	434	pahoehoe lava top	3	Basalt	11.9	1.2
D11	12°23.903'	40°30.777'	449	pahoehoe lava top	5	Basalt	10.1	1.2
D13	12°24.588'	40°31.120'	442	pahoehoe lava top	4.3	Basalt	5.4	0.6
D30	12°22.620'	40°31.848'	473	pahoehoe lava top	5	Basalt	9.6	1.0
D31	12°21.707'	40°31.108'	490	pahoehoe lava top	7	Basalt	9.5	1.0
D32	12°21.530'	40°29.840'	548	<i>pahoehoe lava top</i>	9	<i>Basalt</i>		
D33	12°21.547'	40°27.810'	585	<i>pahoehoe lava top</i>	12	<i>Basalt</i>		
D36	12°28.575'	40°28.957'	367	pahoehoe lava top	5.9	Basalt	10.9	1.1
Rift Axis lavas								
D15	12°23.903'	40°32.742'	436	pahoehoe lava top	2.3	Basalt	21.8	2.2
D17	12°23.783'	40°33.367'	440	pahoehoe lava top	1.4	Basalt	24.4	2.2
D19	12°23.870'	40°33.055'	405	<i>pahoehoe lava top</i>	1.9	<i>Basalt</i>		
D20	12°23.652'	40°33.275'	429	<i>pahoehoe lava core</i>	1.7	<i>Dolerite</i>		
D23	12°23.932'	40°32.795'	396	pahoehoe lava top	2	Basalt	19.6	2.3
D28	12°22.890'	40°33.575'	463	<i>spatter cone</i>	2.4	<i>Basalt</i>		
Cald-1	12°21.157'	40°34.957'	576	pahoehoe lava top	0	Basalt	24.3	2.6
D29	12°22.553'	40°33.448'	495	pahoehoe lava top	0	Basalt	25.0	1.7
D16	12°23.860'	40°33.532'	430	pahoehoe lava top	0	Basalt	7.0	1.1
Gab-C3	12.4834	40.5351	383	pahoehoe lava top	0	Basalt	6.4	1.1

^a The "rift axis" refers here to the middle of the axial valley (dotted line on Fig. 2).

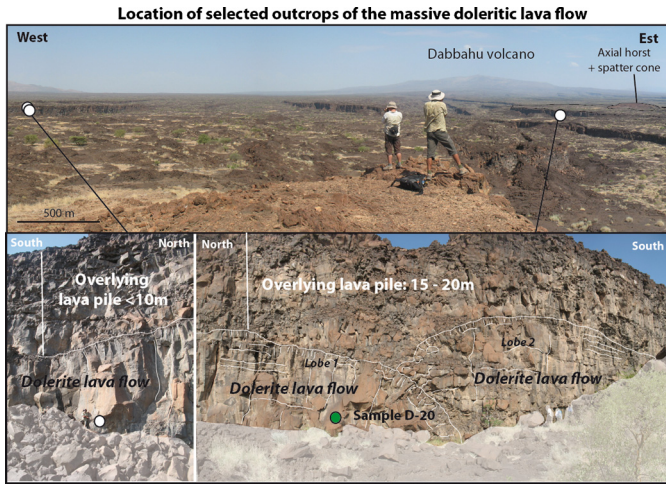


Fig. 3. Top figure shows the orientation of the photo montage, oriented toward the Dabbahu volcano (coordinates: lat. 12°22'51.84"N, long. 40°33'26.39"E), note the eruptive spatter cone on the axial horst. We identified two fault locations (circles) where the same massive doleritic lava unit outcrops, suggesting that its emplacement extends over more than 2 km from the rift axis. This layer is recognizable as shown on the lower photos (the photo on the right corresponds to the sampling site of sample D-20 – coordinates: lat. 12°23'32.02"N, long. 40°33'22.96"E). It is notable that the height of the lava pile overlying this recurrent massive dolerite lava flow diminishes from the rift axis toward its flanks, suggesting an axial emission point (see left photo – coordinates: lat. 12°22'51.30"N, long. 40°33'6.74"E). The recurrence of this pattern seems to be representative of a complete magmatic phase, starting with the dolerite layer, and followed by the emplacement of piled basalt flow fields.

The youngest samples are **Gab-C3** (which was reanalysed for cosmogenic ^{36}Cl after being dated with cosmogenic ^3He by Medynski et al. (2013) and **D-16**, which belongs to the same vol-

canic unit but at its southernmost extremity (Fig. 2). This eruptive unit looks similar to the lavas erupted in 2007, 2009 and 2010, following shallow dike intrusions (Ferguson et al., 2010; Grandin et al., 2010a, 2010b). Although the volumes erupted since 2005 are much smaller than the Gab-C3/D-16 unit, both of these pahoehoe flow fields seem to have involved a similar eruption style, issuing from small aligned eruptive vents suggesting the involvement of a shallow dike.

The oldest samples in the stratigraphic lava pile to be dated were samples **D-15**, **D-17** and **D-23** (see Fig. 2). Sample D-19 was used for chemistry alone.

It should be noted that while most of the flows can be related to a spatter cone in the area, there is no obvious volcanic cone associated with the flow from which D-29 was taken, but the slope variation is more consistent with an origin from the caldera rather than from a fissure within the axial depression.

5. Chronological constraints

While dating lava emissions using cosmogenic nuclide accumulation in lava surfaces is well adapted to this geological and climatological context, only the uppermost lava in a given pile of lavas can be dated. The principles behind cosmogenic nuclide dating (by ^{36}Cl and ^3He) and the techniques used are described in the Supplementary Online materials (SOM 2). The lava surface exposure ages calculated for the mid-segment Dabbahu MRS lava-flows range from 5.4 ± 0.6 ka (D-13) to 24.7 ± 1.6 ka (D-29) (Table 1 and SOM2 Tables 3 and 4). The volcanic stratigraphy established on the basis of these results is summarized in Figs. 2 and 6. A lava flow emplaced on the edge of the depression and currently dissected by the Eastern faults of the depression was dated by the Ar–Ar technique at 30.0 ± 5.4 ka by Ferguson et al. (2013) (sample DF-1 in Fig. 2).

Two main resurfacing events in the axial depression and on the rift western flank can be identified from the ages of the different flows.

5.1. Rift-axis volcanism: a major resurfacing event of the depression at about 25–20 ka

The first major resurfacing event spreads north from the vicinity of the caldera, and took place at about 25–20 ka. Samples Cald-1 and D-29 (that represent the samples closest to the axial caldera – Fig. 2) yield indistinguishable ages (respectively 24.3 ± 2.6 and 25.0 ± 1.7 ka) suggesting a rapid succession of eruptive units. About 5 km north of the caldera stands an eruptive cone (Fig. 2), preserved due to its location on the horst described above. This cone was active coevally with the caldera units, and produced lavas between 24.4 ± 2.2 ka (sample D-17) and 19.6 ± 2.3 (D-23). It is likely that this episode ended with the formation of the caldera, with a rapid emptying of a shallow reservoir. The lavas dated around 24–20 ka in this study share similar geomorphologic characteristics with the 30 ka lavas of the Eastern rift shoulder (Ferguson et al., 2013). The broad spatial distribution of their associated eruptive vents within the rift and the formation of an axial caldera, suggest that this was a major resurfacing event that may have spread over the whole Dabbahu rift segment. This resurfacing event represents a considerable volume of lava for the DMH itself; at least 5 km³ of lava was emitted. This is a minimum estimate because the base of this eruptive episode is not constrained – we estimated an average lava pile height of closely-spaced (temporally and spatially) eruptions of about 20 m for a surface of 280 km².

The youngest activity recorded in the depression consists of lavas that were emplaced at the rift axis at about 6 ka. These younger flows filled the graben on the eastern side (Fig. 2) in the vicinity of eruptive fissure vents, and may represent much smaller lava volumes (less than 100 km² covered with an estimated lava pile thickness of less than 10 m from field observations). These flow fields are clearly identifiable on satellite images as low albedo lava flows, and which, in contrast to the previous resurfacing event (20–25 ka), were clearly flowed up against existing fault scarps.

5.2. Flank volcanism: a recent (<15 ka) resurfacing of the western shoulder of the rift

The second major resurfacing event occurred on the western flank of the rift, at the Durrie volcanic complex. The ages of the various units of the Durrie flank volcano range from 16.3 ± 2.8 ka (D-2) to 5.4 ± 0.6 ka (D-13), coeval with the last resurfacing episode in the rift axis (samples D-16 and Gab-C). Emission of individual lava units was distributed along the different mapped eruptive centres. For instance, the oldest recorded lava flow field (samples D-2 and D-6, dated at 15.0 ± 1.5 ka and 14.9 ± 1.5 ka respectively) spread concentrically away from the main spatter cone, which we interpret as the source of this flow field. The subsequent unit (D-9 and D-14, dated at 11.7 ± 1.2 ka and 11.9 ± 1.2 ka respectively) erupted from an eastern cone that is located ~1 km away from that of the D-2/D-6 flow field. Samples D-30, D-31 and D-1 display similar ages (at 9 ka) and were emitted from small cones to the south-east of the main spatter cone. The last (youngest) lava was erupted at 5.4 ± 0.6 ka (D-13) further north, closer to the rift axis (Fig. 2) and is characterized by thinner and less laterally extensive flows than those related to the main spatter cone (Fig. 2). The widely dispersed eruptive centres (in purple in Fig. 2) associated with volumes of lava <2 km³ strongly suggest that this flank volcanism corresponds to a significant resurfacing event at 15–10 ka. The volume estimation was made based on a

160 km² area covered and an average lava pile height of 10 m. However, the lava volumes could possibly be higher, depending on how the basement topography is estimated: a maximum value of 4 km³ is obtained if we instead use an average pile height of 25 m, a plausible possibility given that some relics of the AVC complex outcrop in the vicinity of the Durrie main spatter cone – Fig. 2, suggesting a shallow basement.

6. Two geochemically distinct magmas present within the same rift segment

Major and trace element concentrations were determined by ICP-OES and ICP-MS respectively, at the Service d'Analyse des Roches et des Minéraux (SARM, CRPG–Nancy, France) following the protocol established by Carignan et al. (2001), either on whole rock material or on separated matrix for phenocryst-bearing lavas. The samples are all sub-alkaline basalts and the variations of some selected major and minor elements are presented in Fig. 4 (for the complete lava compositions see SOM 3).

The axial and flank (Durrie) lavas are chemically distinct, notably with axially erupted lavas being richer in Fe₂O_{3T} and TiO₂, in incompatible elements (except Sr), and depleted in Al₂O₃ for a given MgO content (Fig. 4). The use of compatible elements is particularly appropriate to assess the crystallization sequence occurring within magma chambers; especially Ni that is compatible with olivine and pyroxene, whereas Cr is compatible only with pyroxene. The decrease in Ni correlates perfectly with MgO depletion in both series, while Cr decreases only in axial lavas (Fig. 4); these variations show that only olivine crystallizes in the flank magma chamber, whereas fractionation of both olivine and clinopyroxene occur in the axial magma (Fig. 4). Nevertheless, this crystallization sequence *cannot* account for the differences in Fe₂O_{3T}, TiO₂, and Al₂O₃ between the two (axial and flank) lava series. This major element variability is also associated with variations in trace element concentrations, with axial lavas being slightly enriched in incompatible elements (except Sr) in comparison to flank lavas (e.g. Durrie – Figs. 4, 5). These compositional differences can be most easily attributed to either crustal contamination or to primary liquid differences (different degrees of melting or different mantle domains). An immature, more reactive plumbing system below the flank volcanoes might be expected to result in a greater proportion of crustal contamination at Durrie relative to axial lavas. However, crustal contamination alone cannot account for the observed chemical variations, notably the difference in Fe₂O_{3T} (at a given MgO) is unlikely to result from assimilation of a predominantly felsic crust. Also, contamination via assimilation of previously crystallized and possibly hydrothermally altered basaltic rocks (the most likely lithologies constituting the magma chamber margins) would result in the contaminated melts displaying negative Eu and Sr anomalies (France et al., 2014), which are not observed (Fig. 5). Importantly, the geochemical markers that discriminate axial from flank lavas (Fe, Ti, Al, incompatible elements) also correlate with trace element ratios that are sensitive to the fraction of partial melt in the mantle source region, such as Sm/Yb (Fig. 4). Sm/Yb fractionates in the presence of garnet-bearing mantle, while La/Sm variations can indicate variable degrees of melting of a spinel-bearing mantle. Additionally, a pronounced positive Sr anomaly would mark a contribution from low-pressure plagioclase-bearing mantle. In the present case, flank lavas display strong positive Sr anomalies (while axial lavas display no anomaly), similar La/Sm to axial lavas, and lower Sm/Yb than axial lavas. These results are consistent with higher degrees of melting of a garnet-bearing mantle in the flank lavas, a similar degree of partial melting of spinel-bearing mantle, and an influence of low-pressure plagioclase-bearing mantle present only in

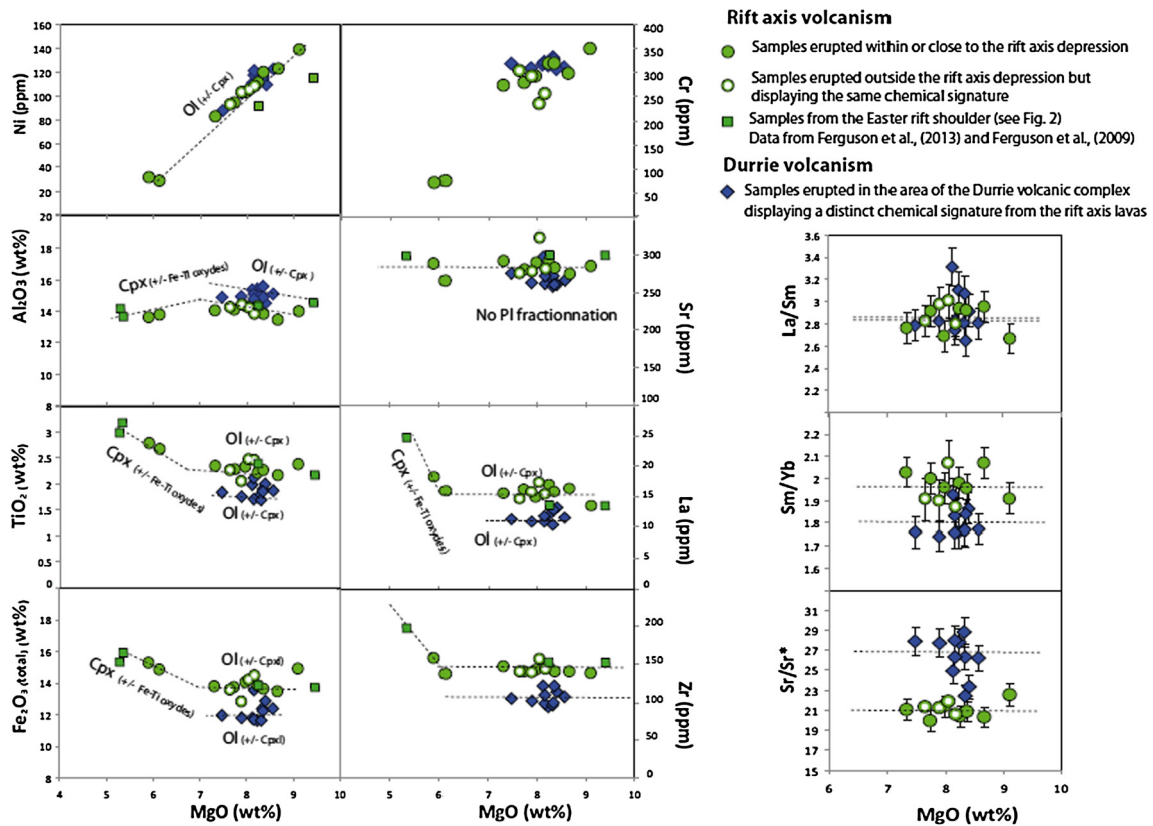


Fig. 4. Chemistry of lava samples. Heavy and light rare earth element (REE) compositions are normalized to E-MORB (Gale et al., 2013). The Sr anomaly (noted Sr*) was calculated after normalizing the trace element ratio to N-MORBs (Gale et al., 2013). $Sr^* = Sr / ((Pr + Nd) / 2)$. Diamonds: samples outcropping on the flank and with flank-affinity chemistry; filled circles: axial samples; empty circles: samples outcropping on the flank but with axial chemical affinity (see text for description of axial and flank chemical affinities).

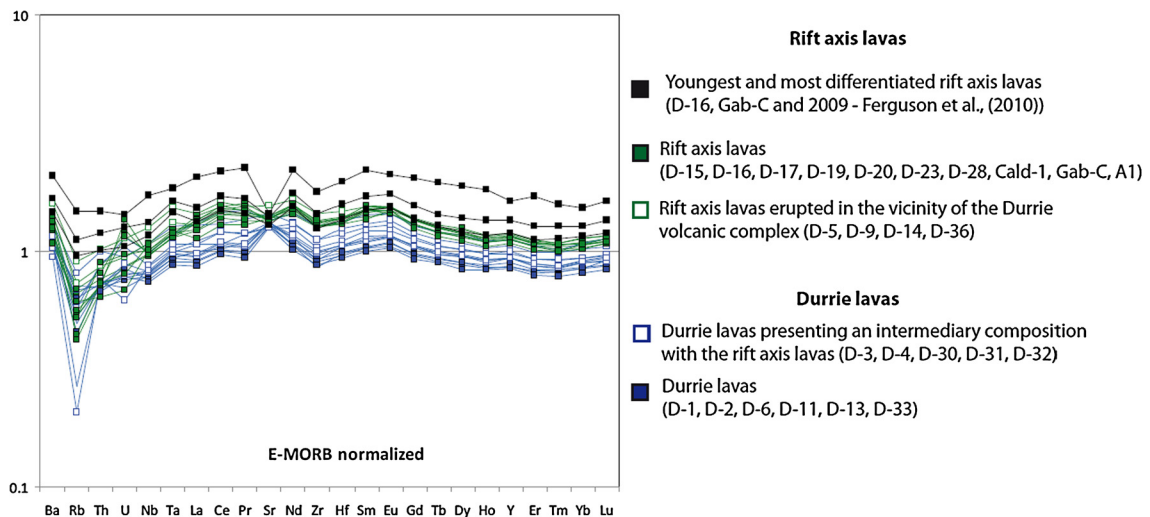


Fig. 5. Spider diagram, normalized to E-MORB (Gale et al., 2013). The youngest lavas (erupted at 6–7 ka and in 2007) are in black and are enriched in incompatible elements compared to the other lavas (from the axis and the flanks) due to their higher degree of differentiation. As expected, the axis lavas (green) display higher values than the flank lavas (blue), due to the higher partial melt fraction occurring beneath the flanks. However, it seems that there is a compositional continuum between the two groups of lavas, illustrated by the blue empty squares of the flank lavas.

the flank lavas (Chalot-Prat et al., 2010). Mantle-derived melts that have equilibrated, at least partially, with plagioclase bearing mantle have been shown to be Al-rich, and poorer in Fe + Ti than mantle melts originated in deeper (spinel- or garnet-bearing) mantle domains (Chalot-Prat et al., 2010), consistent with the differences observed between the flank (influence of plagioclase-bearing mantle), and axial lavas (no influence of plagioclase bearing man-

tle). Higher degrees of partial melting for flank lavas are also consistent with their lower concentration in incompatible elements (Figs. 4, 5).

Given that there is both a higher partial melt fraction derived from deep garnet-bearing mantle and an influence from a shallow plagioclase-bearing mantle in the flank lavas, we expect a larger melting column in the flank area than at the axis. This also implies

that the thermal anomaly is centred slightly to the west of the present day morphological axis (~15 km to the west). These conclusions are consistent with recent magnetotelluric data that image a larger magma body ~15 km to the west of the present day morphological axis (Desissa et al., 2013; Fig. 7).

Thus we conclude that two distinct parental magmas are present in this portion of the DMH, with the flank lavas characterized by slightly higher partial melt fractions of the same mantle source than that implicated in the axial magmatism. The geomorphological and geochronological identification of two distinct volcanic eruptive centres (e.g. the Durrie volcano and the mid-axis magma chamber, Fig. 2), well-separated in space and time, is therefore also supported by their geochemistry. However, a few samples which present a “rift-axis chemical affinity” were actually erupted on the flank (for example, flow field D-9/D-14 and flow field D-36; Fig. 2). Based on this observation, in the following discussion we distinguish flank and rift-axis volcanics on the basis of their composition (Fig. 2), bearing in mind that lavas genetically linked to the rift-axis reservoir can also erupt up to 6 km west of the axis. In addition, some infiltration of axial-type magma into the flank volcanism may have occurred, particularly when looking at the spread of Sr/Sr* in Durrie (flank) volcanic products (Fig. 4).

7. Discussion

7.1. Distribution and longevity of magma reservoirs along the DMH rift

The volcanism encased in the rift axis depression and the western flank volcanism linked with the Durrie volcanic cones were supplied by at least two distinct reservoirs, whose peaks of activity are asynchronous, e.g. the axial reservoir had its maximum input rate around 30–20 ka while the Durrie volcano has been the main source of magmatic activity since 15 ka. This change in the focus of magmatic activity constrains the stability of magma dynamics in space and time, demonstrating that unfocused magmatic activity is a feature on certain time and length scales in the central DMH rift. In this section we examine the distinct stages of volcanism on the flank and in the rift and show that variable magma supply to the surface (in flux and in spatial distribution) is linked to the differentiation and lifetime of discrete magma reservoirs in the crust.

7.1.1. A “dying” axial reservoir

The presence of a magma chamber (the “mid-segment magma chamber”, MSMC) located below the rift axis approximately 1 km south of the caldera (Fig. 1) has been identified from geomechanical modelling of crustal movement following the 2005 dike injection (Grandin et al., 2009; Wright et al., 2006) and from seismicity (e.g. Ebinger et al., 2008). Our rift-axis lavas were likely erupted from this mid-segment magma reservoir. These lavas exhibit a drastic decrease in MgO content since 10 ka (Fig. 6), which probably result from differentiation processes. It appears from the age/composition correlation in Fig. 6 that this reservoir was previously at steady state (i.e. extrusion = supply) due to periodic replenishment balancing lava production. The subsequent period of intense volcanic activity and resurfacing from 25 to 10 ka likely started with the eruption of the more primitive massive doleritic lavas (D20: MgO = 9.2%) that recurrently outcrop at the base of the 20 m thick lava pile throughout the rift axis. This major eruption episode could have triggered the formation of the axial caldera, present directly above the MSMC. However, after 10 ka, the MSMC evolved towards distinctly more differentiated basalts (Fig. 6), most likely associated with a decrease or a permanent break in magma supply from depth.

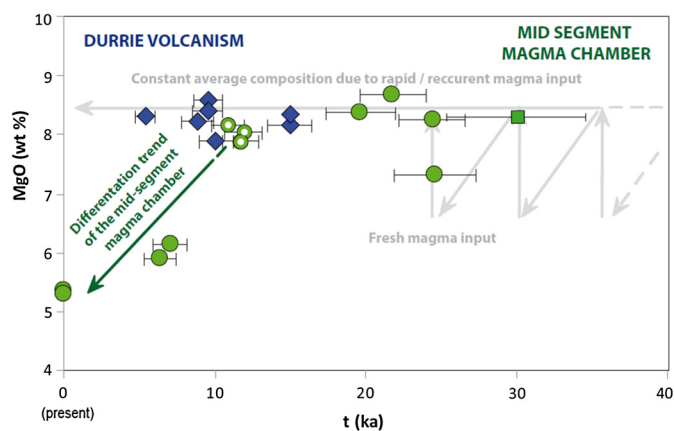


Fig. 6. Magma replenishment and differentiation through time at the rift axis and on the flank (Durrie). Symbols as for Fig. 3. Although the MSMC has been continuously active since at least ~30 ka ago, this diagram illustrates that there was a dramatic change in behaviour at around 10 ka, after which more differentiated lavas were erupted at the axis, indicative of a reduced magma supply to the MSMC. Flank volcanism was first recorded at about 15 ka, by contrast all lava products on the flanks are relatively undifferentiated, indicating a sustained magma supply. Coeval lava emission occurred in the axial depression and on the flank (~15 km to the west) over a period of at least 15 ka.

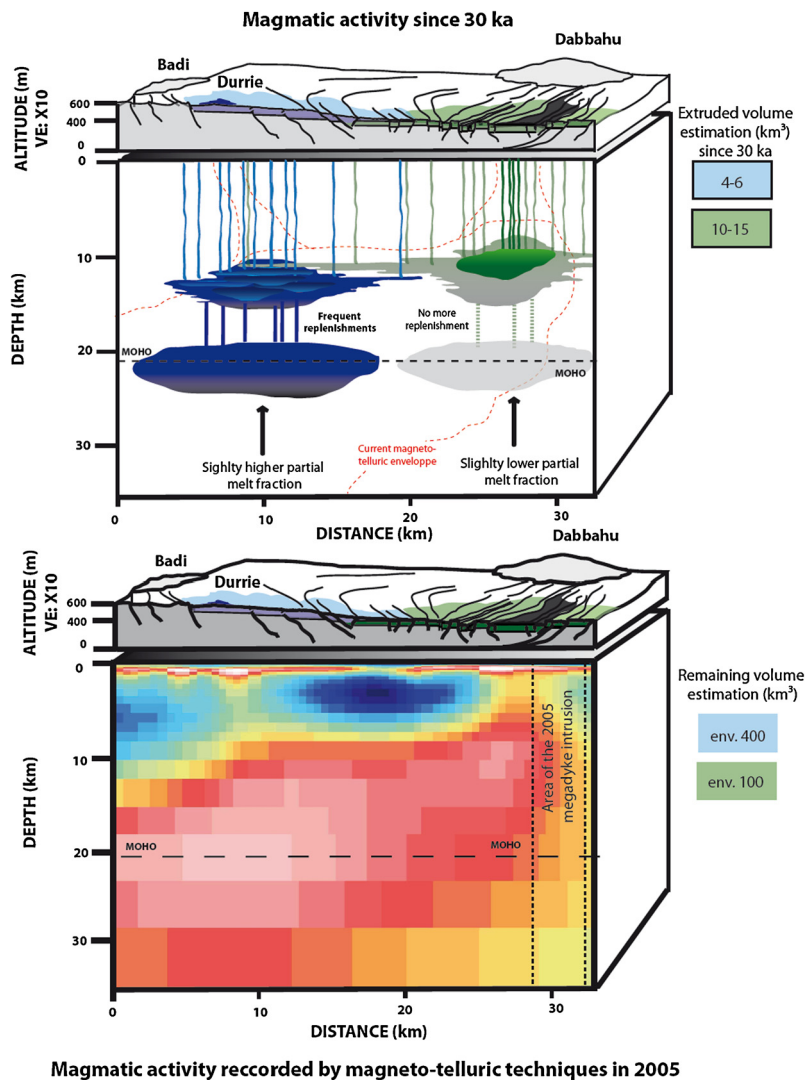
7.1.2. A “fully active” rift flank reservoir

In contrast, chemical variations in lavas erupted on the flank from 14.5 to 5.4 ka are less pronounced. During this time span, MgO content is maintained within a restricted range from 7.9 to 8.6 wt%, equivalent to the composition of axial lavas older than 10 ka. These limited compositional variations over a long period of time reflect the fact that shallow reservoirs have been periodically refilled by more primitive magmas from deeper in the crust or at the crust/mantle boundary. From the perspective of the magmatic cycles described above, this would put the Durrie volcano in a phase of high magma input, with rapid, and possibly frequent magma replenishments (Figs. 6 and 7).

7.1.3. Comparison with present-day magma repartition within the crust

Desissa et al. (2013) collected magnetotelluric data (MT) along the same transect as our samples (Fig. 2). These data indicate a 35 km-wide zone of high electrical conductivity at crustal/upper mantle depths. Using compositional constraints from geochemistry of lava samples and two-phase mixing laws, they deduced that the high conductivity zone contains at least 500 km³ of magma (with up to ~13% of melt). Two magma bodies can be identified from the MT, one located beneath the mid-segment axis and the second located beneath the Durrie volcanic complex on the western rift flank (Fig. 7). Although MT imaging cannot determine whether these two magma bodies are connected, it nevertheless provides strong constraints on the relative volumes and locations of magma that might be available.

Our conclusions are remarkably consistent with the MT imagery (Fig. 7). Indeed, it appears that the volume of magma currently available below the rift axis (i.e. the mid-segment magma chamber) is considerably less than that available below the flank (Fig. 7), consistent with the recent vigorous activity at Durrie that we have documented here. Moreover, this restricted amount of magma below the current neo-volcanic zone is concentrated in the upper crust, whereas it extends down to at least the crust/mantle boundary below the Durrie flank volcanism. Therefore, the most straightforward explanation of the chemical evolution observed in Fig. 6 is that there was a recent deficit in magma supply from depth to the MSMC resulting in more extensive crystallization and increased differentiation of the magmatic products. According to our dating results, this likely occurred around 10 ka. As a result of this crystallization phase, the magma body imaged by MT is presumably



Magmatic activity recorded by magneto-telluric techniques in 2005

Fig. 7. Correspondence between surface topography and sub-surface resistivity (magneto-telluric image and Moho depth from Desissa et al., 2013). The voluminous magma storage zone can be divided into (at least) two reservoirs: a shallow axial magma chamber (which was also identified from data collected during the 2005 crisis) and a slightly deeper reservoir below the western flank volcanic system. Remnant inter-connectivity is still possible between the two reservoirs, consistent with some of the sampled lava compositions which show evidence of mixing between the axial and flank affinities (magneto-telluric cross section and magma volume estimations from Desissa et al., 2013). The sill-shape illustrated for the Durrie reservoir is inspired from Hammond (2014), who showed that the seismic anisotropy observed here is best explained by the presence of magma stored in sills. These MT observation perfectly fit the geochemical observations which predict the presence of a greater melt column (extending to garnet-bearing mantle) beneath the Durrie volcanic complex than beneath the rift axis (spinel-bearing mantle).

smaller than it was at ~25 ka when it was connected with fresh magma stored deeper in the crust. The present day larger magma body, located under the western flank, first appeared to be active at ~15 ka. This demonstrates that such large magma bodies stored at the base of the crust are stable at least for periods of 10–15 ka over which they can sustain and buffer the composition of shallow reservoirs and erupted lavas by frequent replenishment with fresh magma.

A recent seismic study (Hammond, 2014) showed that the reservoirs below the Durrie volcanic centre are most likely sill-shaped. This reservoir geometry is compatible with our model (Fig. 6) and could account for the larger compositional variability observed at Durrie. However, one of the main interpretations of the Hammond et al study was that the present-day axial volcanism is fed from deep off-axis reservoirs whereas, from the chemistry of the different lavas, we show that the axial and flank magmas evolved in separate reservoirs, in agreement with Ferguson et al. (2013). Minor mixing between rift-axis and flank magmas may nevertheless occur, which is consistent with some interconnected plumbing between Durrie and the axis.

7.1.4. Relation with the recent magmato-tectonic activity in the DMH and future evolution

The two magma bodies with vastly different volumes imaged by MT strengthens the idea of a mid-segment reservoir that is magma-starved and that the magma supply has relocated to below the western margin (Fig. 7). Our dating results suggest that this started around 15 ka. This in good agreement with the 2005 rifting event which involved the participation of three magma reservoirs, including the mid-segment magma chamber, beginning with those beneath the volcanic centres of the northern end of the segment (Wright et al., 2006; Grandin et al., 2009; Ayele et al., 2009). This magma injection disrupted the stability of the mid-segment magma chamber, leading to the intrusion of the “mega-dike” (a 60 km long, 6–8 m wide dike that opened in 2005; Wright et al., 2006) from the MSMC. The absence of MSMC replenishment (which would have been seen with InSAR and/or seismic techniques; Hamling et al., 2009) explains why the latest lavas derived from the MSMC (2007 and 2009, Ferguson et al., 2010) are positioned at the end of the continuous differentiation trend ($MgO < 6 \text{ wt\%}$ – Fig. 6), and have not

been rejuvenated to more primitive compositions. If the mid-axis magma chamber continues to evolve as a closed system (without further replenishment of primary magma), the next logical step in the evolution would be eruption of even more differentiated products. This has been frequently observed in the older volcanic activity of Afar (Lahitte et al., 2003). This long term recurrence of alternating basic and acidic products at the same location appears to be a key feature of the organization and maintenance of such active spreading centres on top of stable soft points in the mantle (e.g. areas of the mantle extending over 10s of kilometres, softened by localized melting process; Geoffroy, 2005).

7.2. Morphological evolution along the axis over the past 30 ka due to unfocussed magmatic activity

There have been at least two major resurfacing events during the past 30 ka over the studied transect, spatially distributed between the axial depression and the flank location of the Durrie volcanic cones.

The first major resurfacing event is sourced from the mid-axial magma reservoir. Our cosmogenic exposure ages, combined with the Ar–Ar age from Ferguson et al. (2013) on the eastern margin, show that a voluminous, monotonous lava pile was emplaced before construction of the modern fault-bounded axial valley. This intense magmatic phase took place around 20–25 ka, and likely erased all the pre-existing topography (Fig. 8). Because lavas in the depression are stacked, and cosmogenic dating can only be performed on the latest, currently outcropping lava, it is impossible to say if lava emplacement in the axial depression was continuous between 19 ka and 6 ka, or if there was a hiatus in volcanic activity at the current rift axis. However, based on field observations, the 6 ka event seems to be significantly smaller in terms of volume erupted (although lava thicknesses are not available for this unit).

The second major resurfacing event is due to the flank activity which erased the pre-existing topography, and was also sufficiently intense to build a significant volcanic cone (Figs. 2 and 7). Currently, the flanks of the Durrie volcano are not tectonically dissected, although open fractures have started to develop.

A major implication is that, for the past 15 kyrs at least, magmatism is *not* limited to the axial topographic depression, and asynchronous volcanic activity can be distributed over more than 15 km from it. This contrasts with most mid-ocean ridge models where focussed (<5 km) magma supply is inferred (Macdonald, 2001). This could be due to the fact that the Dabbahu rift is still immature and is not representative of a true oceanic spreading centre. However Standish and Sims (2010) have shown that off-axis magmatism (up to 10 km from the spreading axis) occurred concomitantly with on-axis magmatism at the South West Indian Ridge (SWIR). Our data therefore support the idea that the DMH rift segment is representative of slow oceanic ridge systems, where magma chambers exist for a few tens of kyrs, and can be distributed in a 15–20 km wide zone. The steady state buffered composition of volcanism occurring by the DMH active magmatic reservoirs (7.9–8.6 wt% MgO) is also in good agreement with the composition of magmas evolving in a system controlled by a slow spreading rate with low melt supplies which are uniformly less differentiated than other types of ridge (e.g. fast spreading ridges) but are more likely to retain variations inherited from the underlying mantle (Rubin and Sinton, 2007).

Given that there has been an established magma supply under the western flank of the rift for at least 15 ka, it seems probable that the centre of magmatic accretion is shifting. We speculate that future intrusion of dikes will be focussed where magma is currently most abundant, i.e. 15 km to the west of the present day

axial depression: the central DMH segment is undergoing a minor “ridge-jump”. While the timescales involved are highly debatable, it seems likely that within the next tens of kyrs a new accretionary axis will be in place westward of the present-day recognized “neo-volcanic zone”.

8. Conclusions

In this study, cosmogenic ^{36}Cl and ^3He lava surface exposure dating, combined with field observations, geological mapping and geochemistry, show that the magmatic activity in a 15 km section across the Dabbahu–Manda Hararo segment is sustained by two distinct reservoirs: one beneath the axis and a second lying 15 km to the west beneath the Durrie volcanic complex. The trace element characteristics of these magmas show that they were generated by variable degrees of partial melting of a homogeneous mantle source. The magmas evolved separately in distinct plumbing systems. The axial magma chamber differentiated slowly over time, consistent with a decrease in magma supply between 20 ka and the present day. Conversely, the slightly off-axis (“flank”) reservoir appears to have been regularly supplied with magma since 15 ka, resulting in less variably differentiated lavas. Interconnections between these two reservoirs have occurred, as well as the eruption of lavas displaying an “axial” signature in an off-axis position (Fig. 8). The steady state buffered composition of volcanism emitted on top of the DMH active magmatic reservoirs (7.9–8.6 wt% MgO) is in good agreement with the composition of magmas evolving in a system controlled by slow spreading rate with low melt supplies.

Our data show that magmatism in the DMH segment is not focussed within the current axial depression but instead is spread out over at least 15 km of the western flank. Coeval lava production occurred from volcanoes that were separated by at least 15 km. Magma supply from two different reservoirs is consistent with magneto-telluric observations by Desissa et al. (2013) which show that two magma bodies are present below the segment, with the main magma body currently located below the western flank, precisely where the most voluminous flank volcanism occurs. The axial reservoir only represents 25 km³ of melt, i.e. about 5% of the total (but still 10 times the amount injected during the dyking events in the current crisis e.g. Desissa et al., 2013). However, given the principal magma location (i.e. in a separate reservoir below the western flank, inactive during the 2005 event) it is likely that future dike intrusions (once the current episode has ceased, i.e. all the stress has been relieved) will originate from and close to the Durrie (flank) reservoir, rather than from the axial magma chamber.

We infer that the Durrie reservoir is currently taking over as the principal magma chamber in the mid-segment, while the axial magma chamber (the source of the 2005 diking event) is not being replenished and is therefore dying. As a consequence, the expression of magmatism over a wider area than the present-day depression alone could be an indicator for a future minor ridge jump. At the scale of slow spreading mid-ocean ridges, this could indicate that magma bodies have a lifetime of at least 10–15 ka, and that the continuity of the magmatic activity is maintained by a system of distinct reservoirs broadly distributed between the current axis and the flanks. In return, the long term recurrence of this change in the focus of magmatic activity could control the location of spreading. Therefore, magma distribution and magma chamber longevity appear to be key features of the organization and maintenance of active spreading centres on top of stable soft points in the mantle. These observations of a rift close to the continent–ocean transition provide valuable information for models of mature oceanic ridge development.

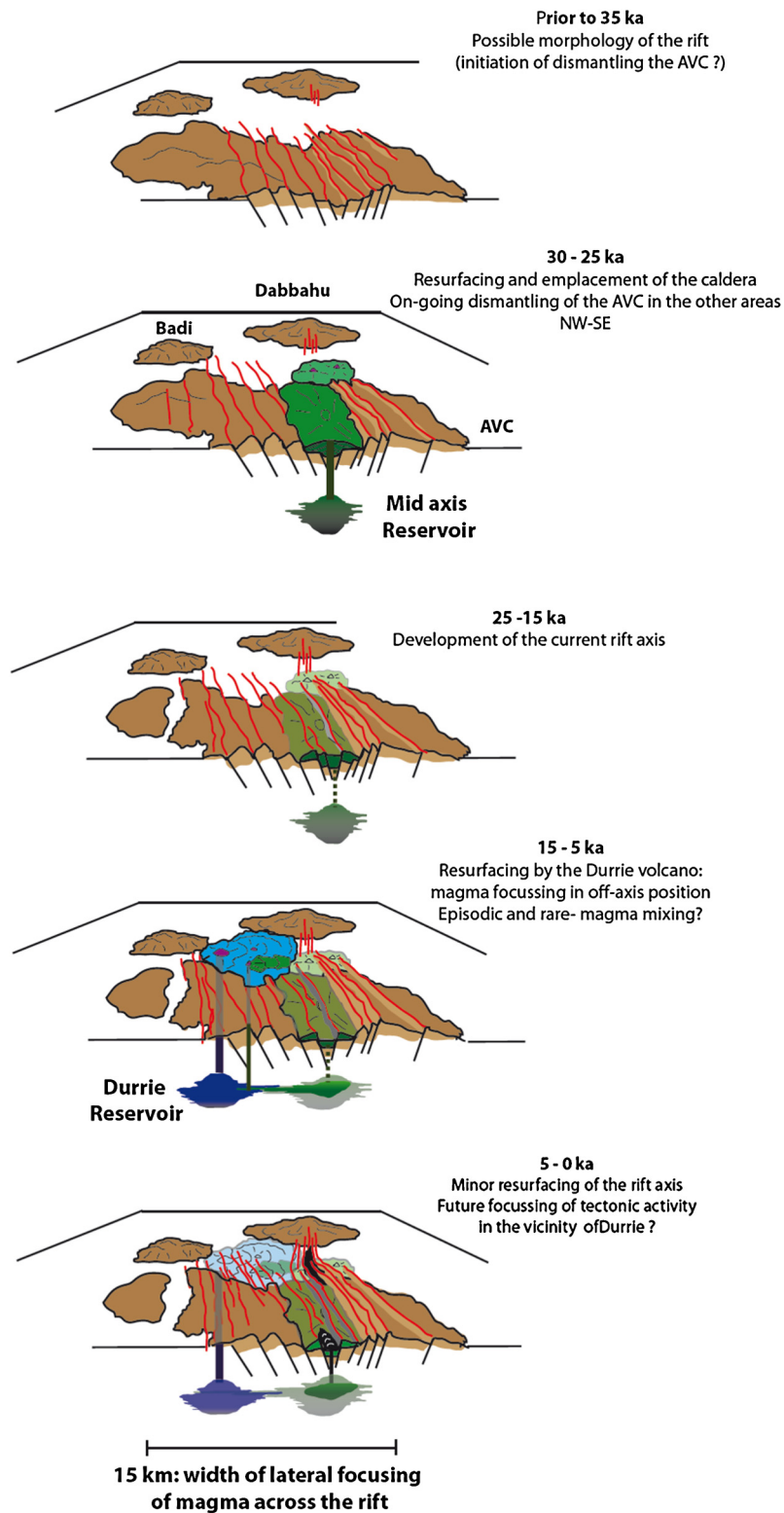


Fig. 8. Schematic evolution of the DMH rift over the past 30 ka illustrating the two main resurfacing events at 30–25 ka (from the mid-axis reservoir) and at 15 ka (from the Durrie reservoir). The evolution of these two magma reservoirs through time suggests relaying magmatic activity from the axis to the western flank, and may prefigure a rift-jump.

Acknowledgements

For their help in the field, we thank the members of the Afar regional government at Semera. We are grateful to B. Tibari (CRPG) for assistance with cosmogenic ³He and U and Th measurements and L. Zimmerman (CRPG) for technical assistance with mass spec-

trometry. We thank Barbara Hoffman for providing the Lidar DEM of the NERC-funded Afar Rift Consortium. CVB publishes with permission of the Executive Director of the British Geological Survey (Natural Environment Research Council). We are very grateful to R. Buck and anonymous reviewer for their constructive review. This is CRPG contribution no. 2345.

Appendix A. Supplementary material

Supplementary material related to this article can be found online at <http://dx.doi.org/10.1016/j.epsl.2014.11.002>.

References

- Ayele, A., Keir, D., et al., 2009. September 2005 mega-dike emplacement in the Manda-Harraro nascent oceanic rift (Afar depression). *Geophys. Res. Lett.* 36 (20).
- Ayele, A., Stuart, G., et al., 2007. The August 2002 earthquake sequence in north Afar: insights into the neotectonics of the Danakil microplate. *J. Afr. Earth Sci.* 48 (2–3), 70–79.
- Barberi, F., Tazieff, H., et al., 1972. Volcanism in the Afar depression: its tectonic and magmatic significance. *Tectonophysics* 15 (1–2), 19–29.
- Bastow, I.D., Keir, D., 2011. The protracted development of the continent–ocean transition in Afar. *Nat. Geosci.* 4, 248–250.
- Bastow, I.D., Nyblade, A.A., et al., 2008. Upper mantle seismic structure beneath the Ethiopian hot spot: rifting at the edge of the African low-velocity anomaly. *Geochem. Geophys. Geosyst.* 9 (12).
- Bastow, I.D., Pilidou, S., et al., 2010. Melt-induced seismic anisotropy and magma assisted rifting in Ethiopia: evidence from surface waves. *Geochem. Geophys. Geosyst.* 11 (6).
- Belachew, M., Ebinger, C., Coté, D., Keir, D., Rowland, J.V., Hammond, J.O.S., Ayele, A., 2011. Comparison of dike intrusions in an incipient seafloor-spreading segment in Afar, Ethiopia: seismicity perspectives. *J. Geophys. Res.* 116, B06405. <http://dx.doi.org/10.1029/2010JB007908>.
- Buck, W.R., 2013. Plate tectonics: magma for 50,000 years. *Nat. Geosci.* 6 (10), 811–812.
- Calais, E.E.C., Hartnady, C., Nocquet, J.M., 2006. Kinematics of the East African Rift from GPS and Earthquake Slip Vector Data.
- Carbotte, S.M., 2005. Seismic structure at mid-ocean ridges. In: Richard, C.S., et al. (Eds.), *Encyclopedia of Geology*. Elsevier, Oxford, pp. 405–417.
- Carignan, J., Hild, P., et al., 2001. Routine analyses of trace element in geological samples using flow injection and low pressure on-line liquid chromatography coupled to ICP-MS: a study of geochemical reference materials BR, DR-N, UB-N, AN-G and GH. *Geostand. News.* 25 (2–3), 187–198.
- Chalot-Prat, F., Falloon, T.J., Green, D.H., Hibberson, W.O., 2010. An experimental study of liquid compositions in equilibrium with plagioclase + spinel Ilherzolute at low pressures (0.75 GPa). *J. Petrol.* 51 (11), 2349–2376. <http://dx.doi.org/10.1093/ptrology/egq060>.
- Colman, A., Sinton, J.M., et al., 2012. Effects of variable magma supply on mid-ocean ridge eruptions: constraints from mapped lava flow fields along the Galapagos Spreading Center. *Geochem. Geophys. Geosyst.* 13, Q08014.
- Desissa, M., Johnson, N.E., et al., 2013. A mantle magma reservoir beneath an incipient mid-ocean ridge in Afar, Ethiopia. *Nat. Geosci.* 6 (10), 861–865.
- Ebinger, C., Ayele, A., et al., 2010. Length and timescales of rift faulting and magma intrusion: the Afar rifting cycle from 2005 to present. *Annu. Rev. Earth Planet. Sci.* 38 (1), 439–466.
- Ebinger, C., Keir, D., Ayele, A., Belachew, M., Calais, E., Wright, T., Campbell, E., Buck, R., 2008. Magma intrusion and faulting processes in a zone of continental rupture: seismicity of the Dabbahu (Afar) rift. *Geophys. J. Int.* <http://dx.doi.org/10.1111/j.1365-246X.2008.03877.x>.
- Ebinger, C.J., Hayward, N.J., 1996. Soft plates and hot spots: views from Afar. *J. Geophys. Res.* 101 (B10), 21859–21876.
- Ferguson, D.J., Barnie, T.D., et al., 2010. Recent rift-related volcanism in Afar, Ethiopia. *Earth Planet. Sci. Lett.* 292 (3–4), 409–418.
- Ferguson, D.J., Calvert, A.T., et al., 2013. Constraining timescales of focused magmatic accretion and extension in the Afar crust using lava geochronology. *Nat. Commun.* 4, 1416.
- Field, L., Blundy, J., et al., 2012. Magma storage conditions beneath Dabbahu Volcano (Ethiopia) constrained by petrology, seismicity and satellite geodesy. *Bull. Volcanol.*, 1–24. <http://dx.doi.org/10.1007/s00445-012-0580-6>.
- Field, L., Blundy, J., et al., 2013. Magmatic history of Dabbahu, a composite volcano in the Afar Rift, Ethiopia. *Geol. Soc. Am. Bull.* 125 (1–2), 128–147.
- France, L., Koepke, J., MacLeod, C.J., Ildefonse, B., Godard, M., Delouie, E., 2014. Contamination of MORB by anatexis of magma chamber roof rocks: constraints from a geochemical study of experimental melts and associated residues. *Lithos* 202–203, 120–137. <http://dx.doi.org/10.1016/j.lithos.2014.05.018>.
- Gale, et al., 2013. *Geochem. Geophys. Geosyst.* 14 (3), 489–518.
- Geoffroy, L., 2005. Volcanic passive margins. *C. R. Géosci.* 337 (16), 1395–1408.
- Grandin, R., Socquet, A., Binet, R., Klinger, Y., Jacques, E., de Chabalière, J.-B., King, G.C.P., Lasserre, C., Tait, S., Tapponnier, P., Delorme, A., Pinzuti, P., 2009. September 2005 Manda Hararo-Dabbahu rifting event, Afar (Ethiopia): constraints provided by geodetic data. *J. Geophys. Res.* 114, B08404. <http://dx.doi.org/10.1029/2008JB005843>.
- Grandin, R., Jacques, E., et al., 2010a. Seismicity during lateral dike propagation: insights from new data in the recent Manda Hararo/Dabbahu rifting episode (Afar, Ethiopia). *Geochem. Geophys. Geosyst.* 12, Q0AB08.
- Grandin, R., Socquet, A., et al., 2010b. Transient rift opening in response to multiple dike injections in the Manda Hararo rift (Afar, Ethiopia) imaged by time-dependent elastic inversion of interferometric synthetic aperture radar data. *J. Geophys. Res.* 115 (B9), B09403.
- Hamling, I.J., Ayele, A., Bennati, L., Calais, E., Ebinger, C.J., Keir, D., Yirgu, G., 2009. Geodetic observations of the ongoing Dabbahu rifting episode: new dyke intrusions in 2006 and 2007. *Geophys. J. Int.* 178 (2), 989–1003.
- Hammond, J.O.S., 2014. Constraining melt geometries beneath the Afar Depression, Ethiopia from teleseismic receiver functions: the anisotropic H- κ stacking technique. *Geochem. Geophys. Geosyst.* 15 (4), 1316–1332.
- Hammond, J.O.S., Kendall, J.M., et al., 2011. The nature of the crust beneath the Afar triple junction: evidence from receiver functions. *Geochem. Geophys. Geosyst.* 12 (12), Q12004.
- Hammond, J.O.S., Kendall, J.M., et al., 2012. The nature of the crust beneath the Afar triple junction: evidence from receiver functions. *Geochem. Geophys. Geosyst.* 12 (12).
- Hayward, N.J., Ebinger, C.J., 1996. Variations in the along-axis segmentation of the Afar Rift system. *Tectonics* 15, 244–257.
- Hofmann, C., Courtillot, V., et al., 1997. Timing of the Ethiopian flood basalt event and implications for plume birth and global change. *Nature* 389, 838–841.
- Keir, D.H., Hamling, I.J., Ayele, A., Calais, E., Ebinger, C., Wright, T., Jacques, E., Mohamed, K., Hammond, J.O.S., Belachew, M., Baker, E., Rowland, J., Lewi, E., Bennati, L., 2009. Evidence for focused magmatic accretion at segment centers from lateral dike injections captured beneath the Red Sea rift in Afar. *Geology* 37, 59–62. <http://dx.doi.org/10.1130/G25147A.1>.
- Keir, Derek, Pagli, Carolina, Bastow, Ian D., Ayele, Atalay, 2011. The magma-assisted removal of Arabia in Afar: evidence from dike injection in the Ethiopian rift captured using InSAR and seismicity. *Tectonics* 30, TC2008. <http://dx.doi.org/10.1029/2010TC002785>.
- Lahitte, P., Gillot, P.-Y., et al., 2003. Silicic central volcanoes as precursors to rift propagation: the Afar case. *Earth Planet. Sci. Lett.* 207 (1–4), 103–116.
- Macdonald, K.C., 2001. Mid-Ocean ridge tectonics, volcanism, and geomorphology. In: John, A., Steele, H., Karl, K.T., Steve, A.T. (Eds.), *Encyclopedia of Ocean Sciences*. second edition. Academic Press, Oxford, pp. 852–866.
- Marty, B., Pik, R.L., et al., 1996. Helium isotopic variations in Ethiopian plume lavas: nature of magmatic sources and limit on lower mantle contribution. *Earth Planet. Sci. Lett.* 144 (1–2), 223–237.
- McClusky, S., Reilinger, R., et al., 2010. Kinematics of the southern Red Sea–Afar Triple Junction and implications for plate dynamics. *Geophys. Res. Lett.* 37 (5), L05301.
- Medynski, S., Pik, R., et al., 2013. Controls on magmatic cycles and development of rift topography of the Manda Hararo segment (Afar, Ethiopia): insights from cosmogenic ^3He investigation of landscape evolution. *Earth Planet. Sci. Lett.* 367, 133–145.
- Pik, R., Marty, B., et al., 2006. How many mantle plumes in Africa? The geochemical point of view. *Chem. Geol.* 226 (3–4), 100–114.
- Rowland, J., Baker, E., et al., 2007. Fault growth at a nascent slow-spreading ridge: 2005 Dabbahu rifting episode, Afar. *Geophys. J. Int.* 171. <http://dx.doi.org/10.1111/j.1365-246X.2007.03584.x>.
- Rubin, K.H., Sinton, J.M., 2007. Inferences on mid-ocean ridge thermal and magmatic structure from MORB compositions. *Earth Planet. Sci. Lett.* 260 (1), 257–276.
- Standish, J.J., Sims, K.W.W., 2010. Young off-axis volcanism along the ultraslow-spreading Southwest Indian Ridge. *Nat. Geosci.* 3 (4), 286–292.
- Tiberi, C., Ebinger, C., Ballu, V., Stuart, G., Oluma, B., 2005. Inverse models of gravity data from the Red Sea–Gulf of Aden–Ethiopian triple junction zone. *Geophys. J. Int.* 163 (2), 775–787. <http://dx.doi.org/10.1111/j.1365-246X.2005.02736.x>.
- Vye-Brown, C., 2012. Geological mapping in the northern part of the Dabbahu Rift Segment, Afar, Ethiopia. BGS Internal Report.
- Vye-Brown, C., Medynski, S., et al., 2012. Geological map of the Dabbahu (Manda-Hararo) Rift, North, 1:100,000 scale. British Geological Survey.
- Vye-Brown, C., Smith, K., Napier, B., Hofmann, B., Wright, T., submitted for publication. Three-dimensional remote mapping of the Afar Rift, Ethiopia. *J. Appl. Volcanol.*
- Wolfenden, E., Ebinger, C., et al., 2005. Evolution of a volcanic rifted margin: Southern Red Sea, Ethiopia. *Geol. Soc. Am. Bull.* 117 (7–8), 846–864.
- Wright, T.J., Ebinger, C., et al., 2006. Magma-maintained rift segmentation at continental rupture in the 2005 Afar dyking episode. *Nature* 442 (7100), 291–294.